JBC Papers in Press. Published on July 31, 2017 as Manuscript M117.795617
The latest version is at http://www.jbc.org/cgi/doi/10.1074/jbc.M117.795617

Modulation of the extent of structural heterogeneity in α-synuclein fibrils by the small molecule thioflavin T

Harish Kumar[‡], Jogender Singh[‡§], Pratibha Kumari[‡¶] and Jayant B. Udgaonkar[‡1]

From the [‡]National Centre for Biological Sciences, Tata Institute of Fundamental Research, Bengaluru 560065, India, the [§]Department of Molecular Genetics and Microbiology, Duke University Medical Center, Durham, NC, 27710, USA and the [¶]ETH Zurich, Physical Chemistry, ETH Honggerberg, 8093 Zurich, Switzerland

Running Title: Thioflavin T modulates the fibrillar heterogeneity

[1]To whom correspondence should be addressed: Jayant B. Udgaonkar, National Centre for Biological Sciences, Tata Institute of Fundamental Research, Bengaluru-560065, India. Tel: 91-80-23666150; Fax: 91-80-23636662; Email: jayant@ncbs.res.in

Keywords: α-synuclein, thioflavin T, fibril heterogeneity, cytotoxicity, hydrogen-exchange, mass-spectrometry

ABSTRACT

The transition of intrinsically disordered, monomeric α-synuclein into β-sheet-rich oligomers and fibrils is associated with multiple neurodegenerative diseases. Fibrillar aggregates possessing distinct structures that differ in their toxicity, have been observed in different pathological phenotypes. Understanding the mechanism of formation of various fibril polymorphs with differing cytotoxic effects, is essential for determining how the aggregation reaction could be modulated to favor non-toxic fibrils over toxic fibrils. In this study, two morphologically different α-synuclein fibrils, one helical and the other ribbon-like, are shown to form together. Surprisingly, a widely-used small molecule for probing aggregation reactions, thioflavin T (ThT), is found to tune the structural heterogeneity found in the fibrils. The ribbon-like fibrils formed in the presence of ThT are found to have a longer structural core than do the helical fibrils formed in the absence of ThT. The ribbon-like fibrils are also more toxic to cells. By facilitating the formation of ribbon-like fibrils over helical fibrils, ThT reduces the extent of fibril polymorphism. This study highlights the role of a small molecule such as ThT in selectively favoring the formation of a specific type of fibril, by binding to aggregates formed early on one of multiple pathways, thereby altering the structural core and external morphology of the fibrils formed.

INTRODUCTION

Conversion of soluble, functionally active proteins into insoluble, β-sheet-rich, aggregated structures is associated with a variety of neurodegenerative diseases such as Parkinson's disease (PD) and Alzheimer's disease (AD) (1–4). Detailed structural analyses of the characteristics of cross β-sheet architecture (5–7) present in these aggregates have revealed their polymorphism (8). It is now known that fibrils formed by a single protein can show multiple distinct conformations under different growth conditions (9–11) as well as under the same growth condition (12–15). The importance of studying fibrillar heterogeneity originated from the prion strain phenomenon, in which a single prion protein is known to cause multiple different pathologies by adopting different types of amyloid like conformations that differ mainly in their external morphologies and molecular structures (16–18). A prion strain propagates a specific pathology faithfully by presenting a specific amyloid template for existing monomer to add on to. Proteins other than the prion protein can also acquire different fibrillar morphologies, which show different levels of toxicity, and propagate faithfully (5, 10). Importantly, fibrils of different morphologies, which differ in their cytotoxicity levels, have been shown to exist in the brains of different AD patients (8, 19). The differences in the toxicity potentials suggest that various fibrils may have different levels of stability, packing and hydrophobicity (20–22). It is now clear that fibril polymorphism is responsible for different pathological phenotypes (23). It is therefore important to understand the origin of fibril polymorphism.

In PD, the central molecular species is the protein α-synuclein, which is an intrinsically disordered protein of 140 residues. It is expressed mainly in the neurons of the central nervous system (CNS), and is found in both soluble and membrane-bound forms in the brain (24–26). It acquires helical and β-hairpin structure, upon binding to membranes and β-wrap proteins, respectively (27, 28). The function of this protein has not yet been ascertained conclusively, although some studies have suggested that it is involved in the process of vesicle release and trafficking (29). α-synuclein is known to aggregate and form Lewy bodies in dopaminergic neurons of the brain. Lewy bodies are made of cross β-sheet-rich structured aggregates called amyloid fibrils, and the process of α-synuclein fibrillation is associated with a variety of neurodegenerative diseases besides PD, including dementia with Lewy bodies (DLBs) (1), AD, and multiple system atrophy (MSA) (2, 3). α-synuclein has been shown to form differently structured amyloid aggregates (10, 12, 13, 15), but there is little understanding of how it does so.

Structural heterogeneity in α-synuclein fibrils originates mainly during the multi-step process of fibrillation, in which monomers self-assemble into various on and off pathway oligomers which vary in their size, shape, structure, stability, and packing (30, 31).

Structurally distinct oligomers appear to grow into different types of fibrillar aggregates whose structural cores resemble the oligomers (31). The structural core of α-synuclein fibrils have been characterized by solid state NMR (ssNMR) (10, 12, 32–34), hydrogen-deuterium exchange mass spectrometry (HDX-MS) (31, 35), HDX-NMR (13, 33), electron paramagnetic resonance (EPR) spectroscopy (36, 37), and proteinase-K treatment (38). Most of the studies indicate that residues 31-109 form the structural core of fibrils (10, 12, 13, 15, 31–38). However, fibrils with a very different structural core, comprised of residues 1-43 and 58-97, have also been characterized (10).

A recent structural model for α-synuclein fibrils, based on solid state NMR, electron microscopy and X-ray fiber diffraction data, suggests a Greek-key topology (32). The atomic structures of fibrils made from peptides corresponding to the NAC and PreNAC segments (residues 68-78 and 47-56, respectively) of the protein, have been characterized in a micro electron diffraction study. Both these sequence segments are present in the structural core of fibrils formed by full length α-synuclein (39). α-synuclein monomers were found to form antiparallel β-sheet structures that stack on top of each other to form a protofilament (39). The protofilaments twist together to form fibrils (39). Cryo-electron microscopy and scanning transmission electron microscopy studies have also been used to characterize the structure of α-synuclein protofibrils. Two protofilaments, each made of three β-strands from the same subunit, form the protofibrils in which sequence segment 8-94 formed the structural core (15). Two protofibrils were found to associate with each other asymmetrically to form fibrils (15). It was hypothesized that the number of protofibrils and their nature of association in the fibrils may determine the final morphology of α-synuclein fibrils and hence, their structural heterogeneity (15).

The process of α-synuclein fibrillation has been described by the nucleation-dependent polymerization (NDP) model which involves a lag phase followed by an exponential phase (40). During the lag phase, monomers undergo structural rearrangements to form transient nuclei, which further grow by the addition of monomers to form fibrils. The molecular structure of the nucleus is likely to determine the molecular structure of the fibrils (41), and modulation of the nucleation and elongation rates by varying growth conditions is expected to modulate the amount of various fibrillar polymorphs (42).

Under different solution conditions, α-synuclein has been shown to form two types of fibrils, which differ in their morphology, structural core, toxicity and infectivity (10). Even under the same aggregation conditions, α-synuclein can form morphologically and structurally different fibrils (12, 13, 15). Understanding the molecular mechanism by which different types of aggregates arise, and how fibril formation can be modulated is crucial for the development of therapeutics for PD and other protein aggregation diseases.

Small molecules have been used extensively for the purpose of modulating and inhibiting the process of aggregation for several disease-linked proteins (43–45), including α-synuclein (46, 47). Binding of small molecules to fibrils can reduce the amount of toxic oligomers by blocking fibril dissociation (48), or by modifying the fibril surface which acts as an efficient catalyst to generate toxic oligomers (49), or by driving the equilibrium towards fibril formation (45). The small molecule thioflavin T (ThT) is used widely to monitor the aggregation process for many proteins due to its ability to bind to cross β-sheet structures found in amyloid fibrils, which modulates its fluorescence properties (50). It is known that ThT binds to different types of fibrils with different affinities (51), and that it can accelerate protein aggregation by binding to monomer or fibrils (52, 53). It is, however, not known whether small molecules such as ThT that bind fibrils can modulate a fibril formation reaction, such that one type of fibrils is preferred over another, or whether the presence of such small molecules during fibril formation can affect the internal structure as well as the external morphology of the fibrils.

In this study, the process of α-synuclein fibrillation in the absence and presence of ThT has been studied. In the absence of ThT, two types of coexisting fibrils were observed. 70% of the fibrils were helical in external morphology and had a shorter structural core, while the remaining 30% of the fibrils had a flat, ribbon-like morphology and had an extended structural core. The addition of ThT during aggregation enhances the rate constant

of α-synuclein fibril formation, and reduces structural heterogeneity with only ribbon-like fibrils being formed.

RESULTS

Effects of ThT on the fibrillation of α-synuclein

To study the effects of ThT on the fibrillation of α-synuclein, 100 μM protein was incubated at pH 7.0, 37 ^{o}C in the absence and presence of 1 mM ThT. The fibrillation process was monitored by measuring the ThT fluorescence emission at 482 nm (Figure 1). In the absence of ThT, fibril formation by α-synuclein followed a NDP mechanism, with a lag phase of ~30 h duration. In contrast, the presence of ThT accelerated the fibrillation of the protein by reducing the lag phase and accelerating the elongation phase. The ThT fluorescence emission signal obtained at saturation for the reaction in the presence of ThT was two-fold higher than for the reaction in the absence of ThT, indicating that either the amount of fibrils was more, or that the fibrils differed in their binding ability to ThT. For fibrils formed in the absence and presence of 1 mM ThT, similar amounts of monomer were found to have converted into fibrils at saturation (Figure S1). Hence, it was likely that the fibrils formed in the absence and presence of 1 mM ThT, differed in their ability to bind ThT.

Effect of ThT on the size and morphology of the fibrils

AFM images were obtained for fibrils formed by 100 μM protein, both in the absence and presence of ThT (Figures 2a and 2b). Two types of fibrils were observed to have formed in the absence of ThT (Figure 2c). One type was helical, with a periodicity of 74 ± 6 nm (Figure 2e), while the other was flat and ribbon-like with no periodicity. The mean heights of the helical and ribbon-like fibrils were 5.7 ± 0.7 nm and 6.3 ± 1.5 nm, respectively. Interestingly, only one type of fibrils was obtained in the presence of ThT; these were flat and ribbon-like with a mean height of 7.4 ± 0.8 nm (Figures 2d and 2f). Similar results were obtained when the fibrils were formed from 50 μM protein. (data not shown). The flat, ribbon-like fibrils formed in the presence of ThT had a larger diameter and less heterogeneity than the flat, ribbon-like fibrils formed in the absence of ThT (Figure 2c and 2d); the standard deviation of the fibril height distribution was 0.8 nm in the former case, and 1.5 nm in the latter case. The difference in the heights of the ribbon-like fibrils formed in the absence and presence of ThT, could conceivably result from intercalation of ThT molecules in the fibrils formed in the presence of ThT.

To check whether the two types of fibrils behave like prion strains, seeds were formed by sonicating the fibrils formed in the absence and presence of ThT, and seeding assays were carried out both in the absence and presence of ThT. It was found that both types of seeds (at 3% concentration) abolished the lag phase regardless of whether ThT was present during the aggregation of 100 μM α-synuclein (Figure S2). Furthermore, the nature of fibrils formed, depended not on the nature of the seed but on whether ThT was present or not during aggregation (data not shown).

Binding of ThT to the fibrils: effect on fibril secondary structure

To determine whether the fibrils made in the presence of ThT, had ThT incorporated into their structure, 100 μM fibrils made in the presence and absence of ThT were incubated with the same concentration (1 mM) of ThT. Free and loosely bound ThT was then removed by washing the fibril pellet with buffer after centrifugation. ThT fluorescence was measured for equal concentrations of the fibrils, to compare the extent of ThT bound to fibrils made in the absence and presence of ThT (Figure 3a). The ThT fluorescence of fibrils made in the presence of ThT was about 5-fold higher than that of the fibrils made in the absence of ThT, but to which ThT was subsequently added. Similar results were obtained when the concentration of associated ThT was determined by measurement of the absorbance at 412 nm (Figure S3a) after first dissolving the fibrils in 8 M GdnHCl. Hence, ThT remained tightly bound to the fibrils made in its presence presumably by intercalating inside the fibrils. These results suggested that the fibrils made in the absence and presence of 1 mM ThT differed in their structures.

To determine if the fibrils made in the presence and absence of ThT differed in their secondary structures, infrared spectra were

acquired (Figures 3b, S3b and S3c). For both fibrils, the presence of the peak near 1630 cm^{-1} suggested that the fibrils had typical parallel β-sheet structures. This peak near 1630 cm^{-1} appeared at a lower wavenumber for the fibrils made in the presence of ThT compared to the fibrils made in the absence of ThT, which suggested an increase in the number of β-strands in the fibrils or a change in the twist angle of the β-sheet in fibrils made in the presence of ThT (54, 55).

Structural characterization of fibrils by hydrogen-deuterium exchange mass spectrometry

HDX-MS was used to further characterize the difference in the internal structures of the fibrils made in the absence and presence of 1 mM ThT. In HDX–MS studies, the amide hydrogen sites that are protected against HDX can be localized to specific segments of the protein sequence by proteolytic fragmentation at low pH, after the HDX reaction is complete. A peptide map of α-synuclein, covering 100% of the sequence, was first generated by controlled proteolysis using pepsin at low pH (Figure S4). The measured mass of each peptide was found to be the same as its calculated mass (Table S1), except for peptide 95-109 whose mass was 18 D less than its calculated mass probably due to water loss. A 5 min labeling pulse was given by incubating the fibrils as well as monomeric protein in deuterated buffer at pH 7.0, 25 ^{o}C. Control samples having no deuteration (0% D) and complete deuteration (95% D) were also run to calculate the amount of deuterium incorporation in different samples (Figure S5). As expected for an intrinsically disordered protein, the monomeric protein showed complete labeling in all of the sequence segments after 5 min of HDX (Figure S6). Regions of the protein which are highly flexible or which remain unfolded in the fibrils would get labeled to the same extent as they do in the monomer. Regions which are part of the structural core of the fibrils would remain protected and not be labeled. In all fibrils obtained under the two different conditions, sequence segments spanning residues 39 to 94 were found to remain highly protected and unlabeled, whereas sequence segments spanning residues 95 to 140 became labeled fully (Figures 4 and S5).

Interestingly, sequence segments spanning residues 1 to 38 showed bimodal mass distributions for the fibrils formed in the absence of ThT, but highly protected unimodal mass distributions for the fibrils formed in the presence of 1 mM ThT (Figure 4). The bimodal mass distributions for the sequence segments spanning residues 1 to 38 indicated the existence of two different conformations differing in structure in this region. One of the conformations showed protection against HDX and hence, was structured, while the other conformation showed no protection against HDX and hence, was not structured in the sequence segment 1-38. Taken together, the data in Figure 4 showed that fibrils formed in the absence of ThT, existed in at least two conformations. One of the conformations had a structured core from residues 1 to 94 while the other conformation had a structured core only from residues 39 to 94 (Figures 5a and 5b). On the other hand, fibrils formed in the presence of 1 mM ThT had only single conformation with a structured core from residues 1 to 94 (Figure 5c).

Differences in molecular structures of fibrils with different morphologies

To correlate the structural core with external morphology for fibrils formed in the absence of ThT, the relative amounts of the two conformations were quantified by fitting the bimodal mass distributions obtained for sequence segments 1-17 and 18-38, to the sum of two Gaussian distributions (Figure 6a). In addition, the fractions of helical and flat fibrils were quantified by counting the numbers of the two types of fibrils from AFM images (Figure 6a). About 70% of the fibrils were found to be helical, while the remaining ~30% fibrils had flat morphology. Interestingly, about 70% of the fibrillar protein molecules had their structural core region extending from residues 39 to 94, while the remaining ~30% of the fibrillar protein molecules had a fibril core that extended from residues 1 to 94. These observations suggested that the helical fibrils are likely to have a core region extending from residues 39 to 94, while the flat, ribbon-like fibrils are likely to have a core region extended from residues 1 to 94. To further establish if the flat, ribbon-like and helical fibrils had core regions extending from residues 1 to 94 and residues 39 to 94, respectively, the structural cores and morphologies of the fibrils were studied at 0.3 mM ThT instead of in the absence of ThT. Importantly,

AFM and HDX-MS studies showed that about 30% of the fibrils were helical in morphology and had a core region extending from residues 39 to 94, and about 70% of them were flat fibrils and had a core region extending from residues 1 to 94 (Figure 6b). Hence, these data suggested that the helical fibrils had a core region extending from residues 39 to 94 and the flat fibrils had a core region extending from residues 1 to 94. These results also suggested that the average helical fibril and the average flat, ribbon-like fibril contained a similar number of protein molecules.

The structure of the N-terminal region was found to differ in the two types of α-synuclein fibrils. In the ribbon-like fibrils but not in the helical fibrils, the N-terminal region was found to be part of the structural core. This suggested that the N-terminal region plays an important role in determining the morphology of the fibrils. Helical fibrils formed in the absence of ThT did not convert into ribbon-like fibrils after incubating the fibrils in 1 mM ThT for 24 h at 25 ^{o}C (data not shown), suggesting that the fibrils have a stable structure and do not interconvert.

Since the presence of ThT modulated fibrillar conformation, it was important to determine how it did so. To this end, α-synuclein aggregation reactions were carried out at different concentrations of ThT ranging from 0 to 1 mM, and AFM imaging was used to determine the relative fraction of helical fibrils formed at each concentration of ThT (Figure 6c). It was seen that the relative fraction of helical fibrils decreased monotonically with an increase in the concentration of ThT present, and that no helical fibrils were seen to have formed at 1 mM ThT concentration. The structure of the final aggregates was also determined using HDX-MS (Figure S7). The relative amounts of the two fibrillar conformations were quantified by fitting the bimodal mass distributions obtained for the sequence segment 18-38 to the sum of multiple Gaussian distributions (Figure S7). Interestingly, the relative amount of fibrillar protein with a core extending from residues 39 to 94, decreased with increasing concentration of ThT (Figures 6c and S7). Thus, the relative amount of helical fibrils decreased from 70% when the fibrillation was carried out in the absence of ThT, to 0% when fibrillation was carried out in the presence of 1 mM ThT. These results showed that ThT reduced structural heterogeneity in the fibrils formed by α-synuclein.

Monitoring the formation of α-synuclein oligomers during fibrillation

To determine whether oligomer formation occurred during the fibril formation reaction carried out in either the absence or presence of ThT, α-synuclein was incubated at two different concentrations (100 μM and 690 μM (10 mg/ml)) under the fibrillation conditions (pH 7.0, 37 ^{o}C) for 5 h. Size exclusion chromatography was used to detect whether oligomers had formed or not. Oligomers were not observed to have formed, both in the absence and presence of ThT (Figure S8a and S8b). Oligomers could only be observed (Figure S8c) when aggregation was carried out at high protein concentration (10 mg/ml) in a different (PBS) buffer at pH 7.4, 37 ^{o}C for 5 h, as described previously (31).

Characterization of the toxicity levels of the fibrils

To determine if the fibrils with different structures were differentially toxic to cells, the toxicities of the fibrils formed in the absence and presence of 1 mM ThT were measured using HEK-293T cells. Equal amounts of fibrils (2.5 μM) were incubated with HEK-293T cells for 24 h, and toxicity was measured using the Wst-1 assay (Figure 7). To eliminate the effect of any free ThT, the fibrils were first washed multiple times with MilliQ water, to remove any free and loosely bound ThT. For toxicity assays, 1 μM ThT was used as a buffer control, and cells without addition of any buffer served as the control. It was found that about 113 ± 22 % of the cells were viable after incubating with fibrils formed in the absence of ThT, whereas about 76 ± 8 % of the cells were viable in the case of fibrils formed in the presence of ThT. It could be concluded that the flat, ribbon-like fibrils formed in the presence of ThT were significantly more toxic to the cells, than the fibrils formed in the absence of ThT. It would therefore appear that fibrils with a flat, ribbon-like morphology are more toxic than fibrils with a helical morphology. Control experiments were carried out to ensure that the observed toxicity was due to fibrils and not due to any free (unbound) ThT. To this end, toxicity assays were carried out at various free ThT concentrations (Figure S9). Free ThT was found to be toxic to

cells at concentrations greater than 1 μM (Figure S9), and not at lower concentrations.

DISCUSSION

The current study focused on understanding the structural and mechanistic basis for heterogeneity in α-synuclein fibrils, and its modulation by the small molecule ThT. In the cases of several neurodegenerative diseases, the aggregating protein concerned was found to adopt distinct fibrillar conformations (5, 8, 15, 19). Thus, understanding the structural and physical basis for fibril heterogeneity may shed light on the different pathological behaviors of distinct fibrillar conformations.

Structural heterogeneity in α-synuclein fibrils and their toxicity levels

In this study, both helical and flat, ribbon-like fibrils were found to form under the same aggregation conditions (Figure 2a and 2c). In a previous study too, α-synuclein was found to form two types of fibrils under a particular aggregation condition, which differed in their secondary structures, morphologies, folds, and the extent and distribution of β-sheets, but which had the same structural core encompassing residues 38 to 95 (12, 13). In contrast, the two types of fibrils observed to form together in the current study had different structural cores (Figure 5a and 5b). The structural core of the helical fibrils is comprised of residues 39 to 94, and that of the flat, ribbon-like fibrils is comprised of residues 1 to 94 (Figure 5a and 5b). Multiple studies using ssNMR (10, 12, 32–34), HDX-MS (31, 35), HDX-NMR (13, 33), EPR spectroscopy (36, 37) and proteinase-K treatment (38) had previously identified the structural core of the α-synuclein fibrils. Most of the studies have identified that residues 31-109 form the structural core of the α-synuclein fibrils (10, 12, 13, 15, 31–38). In a previous study, ribbon-like fibrils were found to form under one aggregation condition, and cylindrical fibrils under another aggregation condition. The two types also differed in their morphology, structural core, toxicity and infectivity (10). The cylindrical fibrils observed in that study resembled the helical fibrils observed in the current study in having a structural core comprised of residues 39 to 94; and the ribbon-like fibrils observed in that study were similar to the ribbon-like fibrils observed in the current study in having a structural core formed by residues 1 to 94 (10). Although the structurally distinct fibrils were shown to differ in their toxicity potentials (10), the properties of fibrils which determine their toxicity potentials are not well known. Factors which are likely to affect fibril toxicity include their stability, their ability to interact with membranes, and their surface hydrophobicity (20–22).

It is seen that the flat, ribbon-like fibrils, which possess the extended structural core, are somewhat more toxic than the helical fibrils (Figure 7). Interestingly, in a previous study, fibrils formed by peptides of two different lengths, which were derived from the α-synuclein NAC (segment 68-78) and SubNAC (segment 69-77) regions, which differed in their structural core, were also found to differ in their cytotoxicity (39). Fibrils made of the longer peptide (NAC), which had a longer structural core, were more cytotoxic than those made by the shorter peptide (39). Further studies are required to delineate the biological importance of the length of the amyloid core.

It is interesting to note that although the fibrils formed in the absence of ThT include flat ribbon-like fibrils similar to those formed in the presence of ThT which are toxic, little if any toxicity was observed for them. It seems that this might be due to the relatively low proportion of ribbon-like fibrils formed in the absence of ThT.

It should be noted that in this study, toxicity was measured after addition of the fibrils to cells for 24 h. It is possible that during this incubation with the cells, the fibrils break down into smaller aggregates, and that it is these smaller aggregates that are toxic. In this context, it should also be noted that oligomers and pre-fibrillar aggregates formed by α-synuclein have been reported to be toxic (56–60), as have been fibrils (10, 61, 62).

Different internal structures lead to different external fibril morphologies

Different fibril morphologies can originate from distinct molecular structures, or from different arrangements of the same molecular structure (6). In the current study, α-synuclein fibrils possessing different morphologies are seen to be made of internal structural cores of different

lengths. It is likely that the fibrils differing in the length of the structural core also differ in extent and organization of β-sheets. The observation that the flat, ribbon-like fibrils with an extended structural core had a larger diameter/height than the helical fibrils (Figure 2c and 2d) suggests that they are likely to have a higher fold symmetry than the helical fibrils, as observed previously for Aβ fibrils (6). In the case of the small protein barstar too, fibrils of very different morphology and diameter, which were, however, formed in different solution conditions, were found to have inner structural cores of different lengths (63, 64). At present, the link between a short structural core and helical fibrillar morphology, and between a longer structural core and flat, ribbon-like fibrillar morphology is not understood in the case of α-synuclein.

Origin of α-synuclein fibril heterogeneity and its reduction by ThT

Structural heterogeneity in α-synuclein fibrils could arise from heterogeneity at the monomer level, which would lead to the formation of distinct nuclei. Due to its intrinsically disordered nature, α-synuclein can adopt various conformations in a given solution condition as characterized by electrospray ionization mass spectrometry (65), single molecule AFM (66), and NMR (67). Modifications in the amino acid sequence and solution conditions have been shown to modulate conformational composition of the ensemble of α-synuclein molecules (66). The conformational diversity could determine the relative proportion of different aggregates that can be formed, as previously suggested for other proteins (23). It can be then expected that stabilization of a specific conformational state upon binding to a small molecule, might lead to the formation of specific aggregates.

Structural heterogeneity in α-synuclein fibrils could also arise from the utilization of multiple pathways for fibril formation. For several other proteins, including barstar (68, 69), and the mouse prion protein (70), structurally distinct amyloid fibrils have been shown to form on different aggregation pathways under different aggregation conditions. In the case of α-synuclein, morphologically and structurally different aggregates have been shown to form from structurally distinct oligomers (31). One oligomer was found to be on pathway to fibril formation, and had a structural core similar to that of fibrils, and the other oligomer with a different structural core grew into amorphous aggregates (31). In the current study, the inability to detect the formation of oligomers during fibril formation under the aggregation conditions used, either in the absence or presence of ThT (see Results and Figure S8), did not permit determination of whether the ribbon-like and helical fibrils arose from structurally distinct oligomers formed on different pathways of fibril formation.

The formation of distinct α-synuclein fibrils suggests that multiple nucleation events can take place under the same aggregation condition. Changes in the aggregation condition may affect the nucleation rate and elongation rate differently for distinct nuclei, which would play an important role in modulating the structural heterogeneity. In the current study, the observation that the presence of ThT accelerates nucleation and elongation (Figure 1), suggests that ThT binds to early species formed during the fibrillation of α-synuclein. Binding of ThT to early aggregates on one pathway when multiple pathways are operative, will stabilize those aggregates, and result in a reduction in fibril heterogeneity.

Role of ThT in modulating the fibril formation reaction of α-synuclein

ThT is known to bind to cross-β-sheet structures found in amyloid fibrils, and has been widely used to monitor the amyloid fibril formation reaction of many proteins (50). The binding of ThT to fibrils can occur in different ways. ThT can bind perpendicular to the long fibril axis, in the cavities formed by the side chains of aromatic/hydrophobic residues across consecutive β-strands on the surface of the β-sheet in the fibrils (51, 71–73). ThT is also known to bind in a parallel orientation to the peptide strand (74). It also appears that ThT can bind to the peptide backbone *via* л- л interactions (75). Hence, it is not surprising that ThT can bind diverse types of amyloid fibrils with different affinities (51). If fibrillar structures (nuclei), which form very early, differ in their binding affinity for ThT, then the early structure (nucleus) that binds most tightly to ThT will be stabilized, and hence, populated the most. The relative amounts of different fibrils formed will reflect the relative

amounts of the initial aggregates (nuclei). Hence, the relative amounts of different fibrils that form will depend on the concentration and binding affinity of the ThT present. Thus, ThT must bind strongly to the early fibrillar structures (nuclei) that lead to the formation of the flat, ribbon-like fibrils. In fact, ThT is seen to remain bound to the final mature flat, ribbon-like fibrils (Figure 3a).

The observation that ThT accelerates the fibrillation of α-synuclein, by increasing the nucleation rate (as indicated in the reduction of the lag phase) (Figure 1), suggests that ThT does indeed bind to early structures (nuclei) formed during the fibrillation process, resulting in an increase in the nucleus concentration, and an increase in the elongation rate. In the case of Aβ, a previous study showed that the nucleation rate was affected more than the elongation rate in the presence of ThT, which also suggests that ThT binds to the early structures on the fibrillation pathway (52, 76).

It is also possible that ThT accelerates the amyloid fibril formation reaction by binding to monomer. In the case of α-synuclein, the electrostatic interaction of ThT with monomeric α-synuclein might favor nucleation, or the conformation conversion of monomer to aggregation-prone structures, which ultimately form the nucleus. Indeed, ThT is known to be able to bind to the negatively charged C-terminus of monomeric α-synuclein (53). Nevertheless, fibrils made from α-synuclein truncated at its C-terminus, can still bind ThT (77), indicating that ThT binds differently to monomer and to fibril.

The C-terminus is known to be the most solvent-exposed region in both oligomers (31, 78, 79) and fibrils (10, 12, 13, 15, 31–38). The C-terminus is also known to stabilize the disordered conformation of the protein by interacting with the N-terminus or NAC domain (80–83). It is likely that the interaction of the C-terminus with the N-terminal region suppresses the participation of the later in forming the structural core of amyloid fibrils (53). Not surprisingly then, C-terminus truncation significantly accelerates the fibrillation of α-synuclein (77, 84). Binding of the C-terminal domain to the NAC region protects the NAC region from participating in aggregation. Binding of the C-terminus to other proteins (85), polyamines (86, 87), and metal ions (9, 88), increases the rate of fibril formation, suggesting that neutralization of negatively charged C-terminus, prevents its binding to the NAC region and N-terminus of the protein. Thus, the interaction of ThT with the C-terminus of α-synuclein might play an important role in modulating the fibrillation reaction.

It should be noted that in this study, a range of ThT concentrations was used to investigate the effect of ThT in modulating structural heterogeneity in α-synuclein fibrils (Figure 6). It was found that fibril formation by α-synuclein was not modulated at ThT concentrations below 30 μM, a concentration which is known to be the critical micelle concentration (CMC) for ThT (89). It seems therefore that structure-modulation by ThT during fibril formation, as seen in this study, is effected by micellar ThT. ThT is used widely for monitoring fibril formation reactions, and the present study suggests that it is safe to do so at concentrations below its CMC.

In summary, the small molecule ThT has been shown to modulate the fibril formation reaction of α-synuclein, and to thereby modulate the structural heterogeneity of the fibrils that form. The presence of ThT during the fibril formation favors the formation of flat, ribbon-like fibrils over the formation of helical fibrils. The flat, ribbon-like fibrils have inner structural core extending from residues 1 to 94, while the helical fibrils have inner structural core extending from residues 39 to 94. The current study highlights the potential use of small molecules in modulating the fibril formation reaction of proteins, so that the less toxic aggregates are favored over the more toxic aggregates.

EXPERIMENTAL PROCEDURES

Protein expression and purification

The plasmid pRK172 containing the human α-synuclein gene was a kind gift from Prof. A. L. Fink. The protein was expressed and purified as described previously (90), with some modification to the procedure. *Escherichia coli* BL21 (DE3) codon plus (Stratagene) cells were transformed with pRK172, were grown overnight at 37 ^{o}C in LB media containing 100 μg/mL ampicillin, and then subcultured into 1000 ml LB containing 100 μg/mL ampicillin. At an OD_{600} of 0.8-1.0 the cells were induced by adding IPTG at a

final concentration of 10 µg/mL, and pelleted down after 5 h. They were resuspended in osmotic shock buffer (30 mM Tris-HCl, 40% w/v sucrose, 2 mM EDTA, pH 7.2), incubated at 25 ^{o}C for 15 min, and centrifuged to remove supernatant. The pellet was resuspended in Milli-Q water containing about 1 mM $MgCl_2$, and the supernatant was obtained after centrifugation. This supernatant was dialyzed twice against 20 mM Tris-HCl buffer, pH 8.0 at 4 ^{o}C. The protein was denatured by adding 8 M urea solution, and loaded on to a DEAE FF ion exchange column (5 ml, HiTrap, GE). The loaded protein was washed, and then eluted out using a gradient of 100 to 300 mM NaCl. Eluted protein was concentrated by ultra filtration (Millipore), flash frozen in liquid N_2, and stored at -80 ^{o}C.

Chemicals, buffers and aggregation condition

All the reagents used were of the highest purity grade available from Sigma Aldrich, unless specified otherwise. GdnHCl was procured from USB (USA). The stored protein was concentrated by filtration using a YM3 filter (Millipore), and denatured in 6 M GdnHCl before injecting into a size exclusion column (Superdex 200 10/300 GL). The protein was eluted out in 20 mM sodium phosphate, 0.01 % sodium azide, 0.1 mM EDTA, pH 7.0 (aggregation buffer), and passed through a YM100 filter to remove any aggregated protein. For aggregation reactions, 500 µl of 100 µM protein were agitated at 750 rpm at 37 ^{o}C (Eppendorf ThermoMixer), in a 1.5 ml centrifuge tube. For aggregation reactions in the presence of ThT, 500 µl of 100 µM protein solution containing 0.01 to 1 mM ThT were agitated at 750 rpm at 37 ^{o}C.

Aggregation studies

Aliquots were withdrawn from the aggregation reaction at various time points, and the amount of fibrils was monitored by measurement of ThT fluorescence at pH 8.0 in 20 mM Tris-HCl buffer. In the assay, 10 µM ThT and 1 µM protein were used. For aggregation reactions carried out in the absence of ThT, 5 µl aliquots were withdrawn and mixed with 495 µl of 20 mM Tris-HCl buffer containing 10 µM ThT. For aggregation reactions carried out in the presence of 1 mM ThT, 5 µl aliquots were withdrawn and mixed with 495 µl of 20 mM Tris-HCl buffer. Then, fluorescence was monitored using a Fluoromax-4 spectrofluorometer, with the excitation and emission wavelengths set at 440 nm and 482 nm, respectively.

Quantification of ThT bound to α-synuclein fibrils

To 45 µl of 100 µM fibrils prepared in the absence of ThT, 4.5 µl of 10 mM ThT were added. To 45 µl of 100 µM fibrils prepared in the presence of 1 mM ThT, 4.5 µl Milli-Q water were added. In both cases, the fibrils were then incubated at 25 ^{o}C for 90 min, and then spun down at 20,000 *g* for 10 min at 9 ^{o}C. The pellet was resuspended in 50 µl of aggregation buffer (without ThT). This was repeated four times to remove the free/loosely bound ThT. Fibril concentration was determined using the BCA assay (kit from Thermo Scientific), and equal amounts of fibrils formed in the absence and presence of ThT were used to monitor the ThT fluorescence, to compare the amount of ThT retained in each fibril sample. The amount of ThT bound to the fibrils was also measured by dissolving the fibrils in 8 M GdnHCl, and monitoring the absorbance at 412 nm.

Atomic force microscopy (AFM)

50 µl of fibrils were applied on to freshly cleaved mica, and incubated for 3 min. The mica surface was rinsed two times with filtered Milli-Q water, and dried under vacuum for 45-60 min. The AFM images were acquired using a FastScan Bio (Bruker) instrument, and analyzed using the WSxM software. The height distribution of the fibrils was obtained by measuring the heights of about 200 fibrils from 10 images of fibrils formed in the presence of ThT, and about 1000 fibrils from 36 images of fibrils formed in the absence of ThT. The nature of the periodicity seen in the helical fibrils was determined by measurements of 32 fibrils from 9 images.

Fourier Transform Infrared (FTIR) spectroscopy

For FTIR measurements, samples were spun down at 20,000 *g* for 10 min at 9 ^{o}C, and fibrils were washed three times with aggregation buffer (without EDTA) made in D_2O, and then resuspended in the same buffer. A thin film was prepared on the diamond crystal by drying 3 µl of sample, using N_2 gas. FTIR spectra were acquired using a Thermo Nicolet 6700 FT-IR spectrometer.

FTIR spectra of the fibrils were analyzed after background subtraction of the spectrum of the appropriate aggregation buffer.

Peptide mapping

To generate a peptide map of α-synuclein, the protein, dissolved in water, was subjected to on-line pepsin digestion in 0.05% formic acid using an immobilized pepsin cartridge (Applied Biosystems) at a flow rate of 50 µL/min on a nanoAcquity UPLC (Waters). The eluted peptides were collected using a peptide trap column (C18 reversed-phase chromatography column), and eluted in to an analytical C18 reversed-phase chromatography column using a gradient of 3–40% acetonitrile (0.1% formic acid) at a flow rate of 45 µL/min. The peptides were directed to the coupled Synapt G2 HD mass spectrometer (Waters). The peptides were sequenced using the MS/tandem MS (MS^E) method, followed by analysis with the Protein Lynx Global Server software (Waters) and manual inspection.

HDX-MS measurements

Fibrils were prepared as described above. 80 µl of 100 µM fibrils were spun down at 20,000 *g* for 20 min at 9 ^oC. The pellet was resuspended in 20 µl aggregation buffer. To initiate deuterium labeling, 10 µl of the above sample were diluted into 190 µl of aggregation buffer (without EDTA) made in D_2O, and incubated at 25 ^oC for 5 min. After a 5 min pulse, 200 µl of the above sample were mixed with 400 µl ice cold quench buffer (0.1 M Glycine-HCl, 8.4 M GdnHCl, pH 2.5), and incubated for 1 min on ice to dissolve the fibrils. The samples were desalted using a Sephadex G-25 HiTrap desalting column equilibrated with water at pH 2.5, using an Akta Basic HPLC. The desalted samples were injected into the HDX module coupled with a nano ACQUITY UPLC system (Waters) for online pepsin digestion using an immobilized pepsin cartridge (Applied Biosystems). Further processing of the sample for mass determination using a Waters Synapt G2 mass spectrometer was carried out as described earlier (91).

Peptide masses were calculated from the centroid of the isotopic envelope using the MassLynx software, and the shift in the mass of labeled peptide relative to the unlabeled peptide was used to determine the extent of deuterium incorporation. As the sample was in 95% D_2O during labeling, and was exposed to H_2O after dissolution in GdnHCl, control experiments were carried out to correct for back-exchange and forward-exchange. To this end, monomeric α-synuclein was completely deuterated by incubating in 20 mM sodium phosphate buffer (pH 7.0) (95% D_2O) at 25 ^oC for 5 min. The fully deuterated α-synuclein sample was then processed in exactly the same way as was the aggregates. The extent of deuterium incorporation in each peptide, % D, was determined using the following equation:

$$\%\, D = (m(t) - m(0\%))/ (m(95\%) - m(0\%)) \times 100 \qquad \text{(Eq. 1)}$$

where $m(t)$ is the measured centroid mass of the peptide at time point t, $m(0\%)$ is the measured mass of an undeuterated reference sample, and $m(95\%)$ is the measured mass of a fully deuterated reference sample (in 95% D_2O) (92).

The percent deuterium incorporation for peptides showing a bimodal distribution was calculated as described earlier (14, 91). The centroid mass for each peak was obtained by fitting the bimodal mass distributions to the sum of two Gaussian distributions using OriginPro 8. % D for each peak was determined using equation 1.

Cytotoxicity assay

Equal concentrations (1 mM) of ThT were added to the fibrils made under the two different conditions and the fibrils were incubated at 25 ^oC for 15 min. The fibrils were spun down at 20,000 *g* for 20 min at 9 ^oC, the supernatant was removed, and the fibrils were washed with an equal volume of autoclaved Milli-Q water. The washing process was repeated three times, and then the fibrils were resuspended in autoclaved Milli-Q water. The concentration of the fibrils was determined using the BCA assay after dissolving the fibrils in 4 M GdnHCl. Equal concentrations (2.5 µM) of fibrils made under the two different conditions were used for the cytotoxicity experiments. Autoclaved Milli-Q water containing 1 µM ThT was used as a buffer control in the cytotoxicity assay. For the assay, HEK-293T cells (human embryonic kidney cells, ATCC) were cultured in DMEM (Gibco) medium supplemented with 10% FBS, at 37 ^oC in a 5% CO_2 humidified environment. Cells were

plated in a 96 well plate at a density of 5000 cells per well to a final volume of 100 µl. After incubation for 25 h, 10 µl of fibrils (25 µM) or only ThT (0.1-5 µM) were added to each well, and the cells were further incubated for 24 h at 37 ^{o}C in 5% CO_2. The Wst-1 assay kit (Roche) was used to measure the viability of the cells. 9 µl of Wst-1 reagent were added into each well, and the cells were incubated for 2.5 h at 37 ^{o}C in 5% CO_2. The optical density at 477 nm was measured with a micro plate reader (Spectramax M5). Data were normalized with respect to data obtained with untreated cells (Control).

ACKNOWLEDGMENTS

We thank members of our laboratory for discussion, and for their comments on the manuscript. We thank Sahil Lall for assistance in carrying out the cytotoxicity experiments, in the laboratory of MK Mathew. The AFM images were collected at the Central Imaging Facility of the National Centre for Biological Sciences. JBU is a recipient of a JC Bose National Fellowship from the Government of India. This work was funded by the Tata Institute of Fundamental Research, and by the Department of Biotechnology, Government of India.

CONFLICT OF INTEREST: The authors declare that they have no conflict of interest with the contents of this article.

AUTHOR CONTRIBUTIONS: H. K., J. S., J. B. U., and P. K. designed the experiments. H. K. performed the experiments. H. K., J. S., and J. B. U. analyzed the results. H. K., J. S., and J. B. U. wrote the manuscript. The final version of the manuscript was approved by all the authors.

REFERENCES

1. Spillantini, M. G., Schmidt, M. L., Lee, V. M., Trojanowski, J. Q., Jakes, R., and Goedert, M. (1997) Alpha-synuclein in Lewy bodies. *Nature*. **388**, 839–840

2. Goedert, M. (2001) Alpha-synuclein and neurodegenerative diseases. *Nat. Rev. Neurosci.* **2**, 492–501

3. Stefani, M., and Dobson, C. M. (2003) Protein aggregation and aggregate toxicity: new insights into protein folding, misfolding diseases and biological evolution. *J. Mol. Med. (Berl).* **81**, 678–99

4. Singh, J., and Udgaonkar, J. B. (2015) Molecular Mechanism of the Misfolding and Oligomerization of the Prion Protein: Current Understanding and Its Implications. *Biochemistry*. **54**, 4431–42

5. Petkova, A. T., Leapman, R. D., Guo, Z., Yau, W.-M., Mattson, M. P., and Tycko, R. (2005) Self-propagating, molecular-level polymorphism in Alzheimer's beta-amyloid fibrils. *Science*. **307**, 262–5

6. Paravastu, A. K., Leapman, R. D., Yau, W., and Tycko, R. (2008) Molecular structural basis for polymorphism in Alzheimer's beta-amyloid fibrils. *Proc. Natl. Acad. Sci. U. S. A.* **105**, 18349–54

7. Fitzpatrick, A. W. P., Debelouchina, G. T., Bayro, M. J., Clare, D. K., Caporini, M. A., Bajaj, V. S., Jaroniec, C. P., Wang, L., Ladizhansky, V., Müller, S. A., MacPhee, C. E., Waudby, C. A., Mott, H. R., De Simone, A., Knowles, T. P. J., Saibil, H. R., Vendruscolo, M., Orlova, E. V,

Griffin, R. G., and Dobson, C. M. (2013) Atomic structure and hierarchical assembly of a cross-β amyloid fibril. *Proc. Natl. Acad. Sci. U. S. A.* **110**, 5468–73

8. Lu, J.-X., Qiang, W., Yau, W.-M., Schwieters, C. D., Meredith, S. C., and Tycko, R. (2013) Molecular structure of β-amyloid fibrils in Alzheimer's disease brain tissue. *Cell*. **154**, 1257–68

9. Hoyer, W., Antony, T., Cherny, D., Heim, G., Jovin, T. M., and Subramaniam, V. (2002) Dependence of alpha-synuclein aggregate morphology on solution conditions. *J. Mol. Biol.* **322**, 383–93

10. Bousset, L., Pieri, L., Ruiz-Arlandis, G., Gath, J., Jensen, P. H., Habenstein, B., Madiona, K., Olieric, V., Böckmann, A., Meier, B. H., and Melki, R. (2013) Structural and functional characterization of two alpha-synuclein strains. *Nat. Commun.* **4**, 2575

11. Otzen, D. E. (2013) *Amyloid fibrils and prefibrillar aggregates: molecular and biological properties*, John Wiley & Sons

12. Heise, H., Hoyer, W., Becker, S., Andronesi, O. C., Riedel, D., and Baldus, M. (2005) Molecular-level secondary structure, polymorphism, and dynamics of full-length alpha-synuclein fibrils studied by solid-state NMR. *Proc. Natl. Acad. Sci. U. S. A.* **102**, 15871–6

13. Vilar, M., Chou, H.-T., Lührs, T., Maji, S. K., Riek-Loher, D., Verel, R., Manning, G., Stahlberg, H., and Riek, R. (2008) The fold of alpha-synuclein fibrils. *Proc. Natl. Acad. Sci. U. S. A.* **105**, 8637–42

14. Singh, J., and Udgaonkar, J. B. (2013) Dissection of conformational conversion events during prion amyloid fibril formation using hydrogen exchange and mass spectrometry. *J. Mol. Biol.* **425**, 3510–21

15. Dearborn, A. D., Wall, J. S., Cheng, N., Heymann, J. B., Kajava, A. V., Varkey, J., Langen, R., and Steven, A. C. (2016) α-Synuclein Amyloid Fibrils with Two Entwined, Asymmetrically Associated Protofibrils. *J. Biol. Chem.* **291**, 2310–8

16. Bessen, R. A., and Marsh, R. F. (1994) Distinct PrP properties suggest the molecular basis of strain variation in transmissible mink encephalopathy. *J. Virol.* **68**, 7859–68

17. Safar, J., Wille, H., Itri, V., Groth, D., Serban, H., Torchia, M., Cohen, F. E., and Prusiner, S. B. (1998) Eight prion strains have PrP(Sc) molecules with different conformations. *Nat. Med.* **4**, 1157–65

18. Stöhr, J., Watts, J. C., Mensinger, Z. L., Oehler, A., Grillo, S. K., DeArmond, S. J., Prusiner, S. B., and Giles, K. (2012) Purified and synthetic Alzheimer's amyloid beta (Aβ) prions. *Proc. Natl. Acad. Sci. U. S. A.* **109**, 11025–30

19. Qiang, W., Yau, W.-M., Lu, J.-X., Collinge, J., and Tycko, R. (2017) Structural variation in amyloid-β fibrils from Alzheimer's disease clinical subtypes. *Nature*. **541**, 217–221

20. Butterfield, S. M., and Lashuel, H. A. (2010) Amyloidogenic protein-membrane interactions: mechanistic insight from model systems. *Angew. Chem. Int. Ed. Engl.* **49**, 5628–54

21. Xue, W.-F., Hellewell, A. L., Hewitt, E. W., and Radford, S. E. (2010) Fibril fragmentation in amyloid assembly and cytotoxicity: when size matters. *Prion*. **4**, 20–5

22. Marshall, K. E., Marchante, R., Xue, W.-F., and Serpell, L. C. (2014) The relationship between

amyloid structure and cytotoxicity. *Prion*. **8**, 192–196

23. Tanaka, M., and Komi, Y. (2015) Layers of structure and function in protein aggregation. *Nat. Chem. Biol.* **11**, 373–7

24. Jao, C. C., Hegde, B. G., Chen, J., Haworth, I. S., and Langen, R. (2008) Structure of membrane-bound alpha-synuclein from site-directed spin labeling and computational refinement. *Proc. Natl. Acad. Sci. U. S. A.* **105**, 19666–71

25. Fauvet, B., Mbefo, M. K., Fares, M.-B., Desobry, C., Michael, S., Ardah, M. T., Tsika, E., Coune, P., Prudent, M., Lion, N., Eliezer, D., Moore, D. J., Schneider, B., Aebischer, P., El-Agnaf, O. M., Masliah, E., and Lashuel, H. A. (2012) α-Synuclein in central nervous system and from erythrocytes, mammalian cells, and Escherichia coli exists predominantly as disordered monomer. *J. Biol. Chem.* **287**, 15345–64

26. Lashuel, H. A., Overk, C. R., Oueslati, A., and Masliah, E. (2013) The many faces of α-synuclein: from structure and toxicity to therapeutic target. *Nat. Rev. Neurosci.* **14**, 38–48

27. Davidson, W. S., Jonas, A., Clayton, D. F., and George, J. M. (1998) Stabilization of alpha-synuclein secondary structure upon binding to synthetic membranes. *J. Biol. Chem.* **273**, 9443–9

28. Mirecka, E. A., Shaykhalishahi, H., Gauhar, A., Akgül, Ş., Lecher, J., Willbold, D., Stoldt, M., and Hoyer, W. (2014) Sequestration of a β-hairpin for control of α-synuclein aggregation. *Angew. Chem. Int. Ed. Engl.* **53**, 4227–30

29. Cabin, D. E., Shimazu, K., Murphy, D., Cole, N. B., Gottschalk, W., McIlwain, K. L., Orrison, B., Chen, A., Ellis, C. E., Paylor, R., Lu, B., and Nussbaum, R. L. (2002) Synaptic vesicle depletion correlates with attenuated synaptic responses to prolonged repetitive stimulation in mice lacking alpha-synuclein. *J. Neurosci.* **22**, 8797–807

30. Lorenzen, N., Nielsen, S. B., Buell, A. K., Kaspersen, J. D., Arosio, P., Vad, B. S., Paslawski, W., Christiansen, G., Valnickova-Hansen, Z., Andreasen, M., Enghild, J. J., Pedersen, J. S., Dobson, C. M., Knowles, T. P. J., and Otzen, D. E. (2014) The role of stable α-synuclein oligomers in the molecular events underlying amyloid formation. *J. Am. Chem. Soc.* **136**, 3859–68

31. Paslawski, W., Mysling, S., Thomsen, K., Jørgensen, T. J. D., and Otzen, D. E. (2014) Co-existence of two different α-synuclein oligomers with different core structures determined by hydrogen/deuterium exchange mass spectrometry. *Angew. Chem. Int. Ed. Engl.* **53**, 7560–3

32. Tuttle, M. D., Comellas, G., Nieuwkoop, A. J., Covell, D. J., Berthold, D. A., Kloepper, K. D., Courtney, J. M., Kim, J. K., Barclay, A. M., Kendall, A., Wan, W., Stubbs, G., Schwieters, C. D., Lee, V. M. Y., George, J. M., and Rienstra, C. M. (2016) Solid-state NMR structure of a pathogenic fibril of full-length human α-synuclein. *Nat. Struct. Mol. Biol.* **23**, 409–15

33. Cho, M.-K., Kim, H.-Y., Fernandez, C. O., Becker, S., and Zweckstetter, M. (2011) Conserved core of amyloid fibrils of wild type and A30P mutant α-synuclein. *Protein Sci.* **20**, 387–95

34. Heise, H., Celej, M. S., Becker, S., Riedel, D., Pelah, A., Kumar, A., Jovin, T. M., and Baldus, M. (2008) Solid-state NMR reveals structural differences between fibrils of wild-type and disease-related A53T mutant alpha-synuclein. *J. Mol. Biol.* **380**, 444–50

35. Del Mar, C., Greenbaum, E. a, Mayne, L., Englander, S. W., and Woods, V. L. (2005) Structure and properties of alpha-synuclein and other amyloids determined at the amino acid level. *Proc.*

Natl. Acad. Sci. U. S. A. **102**, 15477–82

36. Der-Sarkissian, A., Jao, C. C., Chen, J., and Langen, R. (2003) Structural organization of alpha-synuclein fibrils studied by site-directed spin labeling. *J. Biol. Chem.* **278**, 37530–5

37. Chen, M., Margittai, M., Chen, J., and Langen, R. (2007) Investigation of alpha-synuclein fibril structure by site-directed spin labeling. *J. Biol. Chem.* **282**, 24970–9

38. Miake, H., Mizusawa, H., Iwatsubo, T., and Hasegawa, M. (2002) Biochemical characterization of the core structure of alpha-synuclein filaments. *J. Biol. Chem.* **277**, 19213–9

39. Rodriguez, J. A., Ivanova, M. I., Sawaya, M. R., Cascio, D., Reyes, F. E., Shi, D., Sangwan, S., Guenther, E. L., Johnson, L. M., Zhang, M., Jiang, L., Arbing, M. A., Nannenga, B. L., Hattne, J., Whitelegge, J., Brewster, A. S., Messerschmidt, M., Boutet, S., Sauter, N. K., Gonen, T., and Eisenberg, D. S. (2015) Structure of the toxic core of α-synuclein from invisible crystals. *Nature*. **525**, 486–90

40. Wood, S. J., Wypych, J., Steavenson, S., Louis, J. C., Citron, M., and Biere, A. L. (1999) alpha-synuclein fibrillogenesis is nucleation-dependent. Implications for the pathogenesis of Parkinson's disease. *J. Biol. Chem.* **274**, 19509–12

41. Tycko, R. (2014) Physical and structural basis for polymorphism in amyloid fibrils. *Protein Sci.* **23**, 1528–39

42. Qiang, W., Kelley, K., and Tycko, R. (2013) Polymorph-specific kinetics and thermodynamics of β-amyloid fibril growth. *J. Am. Chem. Soc.* **135**, 6860–71

43. Bieschke, J., Herbst, M., Wiglenda, T., Friedrich, R. P., Boeddrich, A., Schiele, F., Kleckers, D., Lopez del Amo, J. M., Grüning, B. a, Wang, Q., Schmidt, M. R., Lurz, R., Anwyl, R., Schnoegl, S., Fändrich, M., Frank, R. F., Reif, B., Günther, S., Walsh, D. M., and Wanker, E. E. (2011) Small-molecule conversion of toxic oligomers to nontoxic β-sheet-rich amyloid fibrils. *Nat. Chem. Biol.* **8**, 93–101

44. Jameson, L. P., Smith, N. W., and Dzyuba, S. V. (2012) Dye-binding assays for evaluation of the effects of small molecule inhibitors on amyloid (aβ) self-assembly. *ACS Chem. Neurosci.* **3**, 807–19

45. Jiang, L., Liu, C., Leibly, D., Landau, M., Zhao, M., Hughes, M. P., and Eisenberg, D. S. (2013) Structure-based discovery of fiber-binding compounds that reduce the cytotoxicity of amyloid beta. *Elife*. **2**, e00857

46. Ehrnhoefer, D. E., Bieschke, J., Boeddrich, A., Herbst, M., Masino, L., Lurz, R., Engemann, S., Pastore, A., and Wanker, E. E. (2008) EGCG redirects amyloidogenic polypeptides into unstructured, off-pathway oligomers. *Nat. Struct. Mol. Biol.* **15**, 558–66

47. Bieschke, J., Russ, J., Friedrich, R. P., Ehrnhoefer, D. E., Wobst, H., Neugebauer, K., and Wanker, E. E. (2010) EGCG remodels mature alpha-synuclein and amyloid-beta fibrils and reduces cellular toxicity. *Proc. Natl. Acad. Sci. U. S. A.* **107**, 7710–5

48. Lam, H. T., Graber, M. C., Gentry, K. A., and Bieschke, J. (2016) Stabilization of α-Synuclein Fibril Clusters Prevents Fragmentation and Reduces Seeding Activity and Toxicity. *Biochemistry*. **55**, 675–85

49. Cohen, S. I. A., Arosio, P., Presto, J., Kurudenkandy, F. R., Biverstål, H., Dolfe, L., Dunning, C.,

Yang, X., Frohm, B., Vendruscolo, M., Johansson, J., Dobson, C. M., Fisahn, A., Knowles, T. P. J., and Linse, S. (2015) A molecular chaperone breaks the catalytic cycle that generates toxic Aβ oligomers. *Nat. Struct. Mol. Biol.* **22**, 207–13

50. LeVine, H. (1993) Thioflavine T interaction with synthetic Alzheimer's disease beta-amyloid peptides: detection of amyloid aggregation in solution. *Protein Sci.* **2**, 404–10

51. Biancalana, M., Makabe, K., Koide, A., and Koide, S. (2009) Molecular mechanism of thioflavin-T binding to the surface of beta-rich peptide self-assemblies. *J. Mol. Biol.* **385**, 1052–63

52. D'Amico, M., Di Carlo, M. G., Groenning, M., Militello, V., Vetri, V., and Leone, M. (2012) Thioflavin T Promotes Aβ(1-40) Amyloid Fibrils Formation. *J. Phys. Chem. Lett.* **3**, 1596–601

53. Coelho-Cerqueira, E., Pinheiro, A. S., and Follmer, C. (2014) Pitfalls associated with the use of Thioflavin-T to monitor anti-fibrillogenic activity. *Bioorg. Med. Chem. Lett.* **24**, 3194–8

54. Chirgadze, Y. N., and Nevskaya, N. A. (1976) Infrared spectra and resonance interaction of amide-I vibration of the antiparallel-chain pleated sheet. *Biopolymers*. **15**, 607–25

55. Zandomeneghi, G., Krebs, M. R. H., McCammon, M. G., and Fändrich, M. (2004) FTIR reveals structural differences between native beta-sheet proteins and amyloid fibrils. *Protein Sci.* **13**, 3314–21

56. Winner, B., Jappelli, R., Maji, S. K., Desplats, P. A., Boyer, L., Aigner, S., Hetzer, C., Loher, T., Vilar, M., Campioni, S., Tzitzilonis, C., Soragni, A., Jessberger, S., Mira, H., Consiglio, A., Pham, E., Masliah, E., Gage, F. H., and Riek, R. (2011) In vivo demonstration that alpha-synuclein oligomers are toxic. *Proc. Natl. Acad. Sci. U. S. A.* **108**, 4194–9

57. Cremades, N., Cohen, S. I. A., Deas, E., Abramov, A. Y., Chen, A. Y., Orte, A., Sandal, M., Clarke, R. W., Dunne, P., Aprile, F. A., Bertoncini, C. W., Wood, N. W., Knowles, T. P. J., Dobson, C. M., and Klenerman, D. (2012) Direct observation of the interconversion of normal and toxic forms of α-synuclein. *Cell*. **149**, 1048–1059

58. Danzer, K. M., Haasen, D., Karow, A. R., Moussaud, S., Habeck, M., Giese, A., Kretzschmar, H., Hengerer, B., and Kostka, M. (2007) Different species of alpha-synuclein oligomers induce calcium influx and seeding. *J. Neurosci.* **27**, 9220–32

59. Conway, K. a, Lee, S. J., Rochet, J. C., Ding, T. T., Harper, J. D., Williamson, R. E., and Lansbury, P. T. (2000) Accelerated oligomerization by Parkinson's disease linked alpha-synuclein mutants. *Ann. N. Y. Acad. Sci.* **920**, 42–5

60. Conway, K. a, Lee, S. J., Rochet, J. C., Ding, T. T., Williamson, R. E., and Lansbury, P. T. (2000) Acceleration of oligomerization, not fibrillization, is a shared property of both alpha-synuclein mutations linked to early-onset Parkinson's disease: implications for pathogenesis and therapy. *Proc. Natl. Acad. Sci. U. S. A.* **97**, 571–6

61. Pieri, L., Madiona, K., Bousset, L., and Melki, R. (2012) Fibrillar α-synuclein and huntingtin exon 1 assemblies are toxic to the cells. *Biophys. J.* **102**, 2894–905

62. Peelaerts, W., Bousset, L., Van der Perren, A., Moskalyuk, A., Pulizzi, R., Giugliano, M., Van den Haute, C., Melki, R., and Baekelandt, V. (2015) α-Synuclein strains cause distinct synucleinopathies after local and systemic administration. *Nature*. **522**, 340–4

63. Kumar, S., Mohanty, S. K., and Udgaonkar, J. B. (2007) Mechanism of formation of amyloid

protofibrils of barstar from soluble oligomers: evidence for multiple steps and lateral association coupled to conformational conversion. *J. Mol. Biol.* **367**, 1186–204

64. Sekhar, A., and Udgaonkar, J. B. (2011) Fluoroalcohol-induced modulation of the pathway of amyloid protofibril formation by barstar. *Biochemistry*. **50**, 805–19

65. Frimpong, A. K., Abzalimov, R. R., Uversky, V. N., and Kaltashov, I. A. (2010) Characterization of intrinsically disordered proteins with electrospray ionization mass spectrometry: conformational heterogeneity of alpha-synuclein. *Proteins*. **78**, 714–22

66. Sandal, M., Valle, F., Tessari, I., Mammi, S., Bergantino, E., Musiani, F., Brucale, M., Bubacco, L., and Samorì, B. (2008) Conformational equilibria in monomeric alpha-synuclein at the single-molecule level. *PLoS Biol.* **6**, e6

67. Gurry, T., Ullman, O., Fisher, C. K., Perovic, I., Pochapsky, T., and Stultz, C. M. (2013) The dynamic structure of α-synuclein multimers. *J. Am. Chem. Soc.* **135**, 3865–72

68. Kumar, S., and Udgaonkar, J. B. (2009) Structurally distinct amyloid protofibrils form on separate pathways of aggregation of a small protein. *Biochemistry*. **48**, 6441–9

69. Sekhar, A., and Udgaonkar, J. B. (2011) Fluoroalcohol-induced modulation of the pathway of amyloid protofibril formation by barstar. *Biochemistry*. **50**, 805–819

70. Jain, S., and Udgaonkar, J. B. (2010) Salt-induced modulation of the pathway of amyloid fibril formation by the mouse prion protein. *Biochemistry*. **49**, 7615–24

71. Krebs, M. R. H., Bromley, E. H. C., and Donald, A. M. (2005) The binding of thioflavin-T to amyloid fibrils: localisation and implications. *J. Struct. Biol.* **149**, 30–7

72. Wu, C., Biancalana, M., Koide, S., and Shea, J.-E. (2009) Binding modes of thioflavin-T to the single-layer beta-sheet of the peptide self-assembly mimics. *J. Mol. Biol.* **394**, 627–33

73. Ivancic, V. A., Ekanayake, O., and Lazo, N. D. (2016) Binding Modes of Thioflavin T on the Surface of Amyloid Fibrils Studied by NMR. *Chemphyschem*. **17**, 2461–4

74. Mao, X., Guo, Y., Wang, C., Zhang, M., Ma, X., Liu, L., Niu, L., Zeng, Q., Yang, Y., and Wang, C. (2011) Binding modes of thioflavin T molecules to prion peptide assemblies identified by using scanning tunneling microscopy. *ACS Chem. Neurosci.* **2**, 281–7

75. Rodríguez-Rodríguez, C., Rimola, A., Rodríguez-Santiago, L., Ugliengo, P., Alvarez-Larena, A., Gutiérrez-de-Terán, H., Sodupe, M., and González-Duarte, P. (2010) Crystal structure of thioflavin-T and its binding to amyloid fibrils: insights at the molecular level. *Chem. Commun. (Camb).* **46**, 1156–8

76. Lin-ling, Y. U., and Yan-jiao, Z. (2016) Dual Effect of Thioflavin T on the Nucleation Kinetics of. 10.3866/PKU.WHXB201603221

77. Hoyer, W., Cherny, D., Subramaniam, V., and Jovin, T. M. (2004) Impact of the acidic C-terminal region comprising amino acids 109-140 on alpha-synuclein aggregation in vitro. *Biochemistry*. **43**, 16233–42

78. van Rooijen, B. D., van Leijenhorst-Groener, K. A., Claessens, M. M. A. E., and Subramaniam, V. (2009) Tryptophan fluorescence reveals structural features of alpha-synuclein oligomers. *J. Mol. Biol.* **394**, 826–33

79. Mysling, S., Betzer, C., Jensen, P. H., and Jorgensen, T. J. D. (2013) Characterizing the dynamics of α-synuclein oligomers using hydrogen/deuterium exchange monitored by mass spectrometry. *Biochemistry*. **52**, 9097–103

80. Okazaki, H., Ohori, Y., Komoto, M., Lee, Y.-H., Goto, Y., Tochio, N., and Nishimura, C. (2013) Remaining structures at the N- and C-terminal regions of alpha-synuclein accurately elucidated by amide-proton exchange NMR with fitting. *FEBS Lett.* **587**, 3709–14

81. Wu, K.-P., and Baum, J. (2010) Detection of transient interchain interactions in the intrinsically disordered protein alpha-synuclein by NMR paramagnetic relaxation enhancement. *J. Am. Chem. Soc.* **132**, 5546–7

82. Losasso, V., Pietropaolo, A., Zannoni, C., Gustincich, S., and Carloni, P. (2011) Structural role of compensatory amino acid replacements in the α-synuclein protein. *Biochemistry*. **50**, 6994–7001

83. Dedmon, M. M., Lindorff-Larsen, K., Christodoulou, J., Vendruscolo, M., and Dobson, C. M. (2005) Mapping long-range interactions in alpha-synuclein using spin-label NMR and ensemble molecular dynamics simulations. *J. Am. Chem. Soc.* **127**, 476–7

84. Burré, J., Sharma, M., and Südhof, T. C. (2012) Systematic mutagenesis of α-synuclein reveals distinct sequence requirements for physiological and pathological activities. *J. Neurosci.* **32**, 15227–42

85. Meuvis, J., Gerard, M., Desender, L., Baekelandt, V., and Engelborghs, Y. (2010) The conformation and the aggregation kinetics of α-synuclein depend on the proline residues in its C-terminal region. *Biochemistry*. **49**, 9345–52

86. Fernández, C. O., Hoyer, W., Zweckstetter, M., Jares-Erijman, E. A., Subramaniam, V., Griesinger, C., and Jovin, T. M. (2004) NMR of alpha-synuclein-polyamine complexes elucidates the mechanism and kinetics of induced aggregation. *EMBO J.* **23**, 2039–46

87. Bertoncini, C. W., Jung, Y.-S., Fernandez, C. O., Hoyer, W., Griesinger, C., Jovin, T. M., and Zweckstetter, M. (2005) Release of long-range tertiary interactions potentiates aggregation of natively unstructured alpha-synuclein. *Proc. Natl. Acad. Sci. U. S. A.* **102**, 1430–5

88. Uversky, V. N., Li, J., and Fink, A. L. (2001) Metal-triggered structural transformations, aggregation, and fibrillation of human alpha-synuclein. A possible molecular NK between Parkinson's disease and heavy metal exposure. *J. Biol. Chem.* **276**, 44284–96

89. Sabaté, R., Lascu, I., and Saupe, S. J. (2008) On the binding of Thioflavin-T to HET-s amyloid fibrils assembled at pH 2. *J. Struct. Biol.* **162**, 387–96

90. Huang, C., Ren, G., Zhou, H., and Wang, C. (2005) A new method for purification of recombinant human alpha-synuclein in Escherichia coli. *Protein Expr. Purif.* **42**, 173–177

91. Singh, J., Sabareesan, A. T., Mathew, M. K., and Udgaonkar, J. B. (2012) Development of the structural core and of conformational heterogeneity during the conversion of oligomers of the mouse prion protein to worm-like amyloid fibrils. *J. Mol. Biol.* **423**, 217–31

92. Zhang, Z., and Smith, D. L. (1993) Determination of amide hydrogen exchange by mass spectrometry: a new tool for protein structure elucidation. *Protein Sci.* **2**, 522–31

FOOTNOTES

[1]To whom correspondence should be addressed: Jayant B. Udgaonkar, Department of Biophysics, Biochemistry and Bioinformatics, National Centre for Biological Sciences, Tata Institute of Fundamental Research, Bengaluru-560065, India.Tel: 91-80-23666150; Fax: 91-80-23636662; Email: jayant@ncbs.res.in

[2]This work was funded by the Tata Institute of Fundamental Research and by the Department of Science and Technology, Government of India. JBU is a recipient of a J.C. Bose National Fellowship from the Government of India.

[3]The abbreviations used are: PD, Parkinson's disease; AD, Alzheimer's disease; MSA, multiple system atrophy; DLBs, dementia with Lewy bodies; LB, Luria-Bertani; Aβ, amyloid beta; HDX, hydrogen-deuterium exchange; MS, mass spectrometry; AFM, atomic force microscopy; ThT, thioflavin T; FTIR, Fourier Transform Infrared; GdnHCl, guanidine hydrochloride;

FIGURES AND FIGURE LEGENDS

FIGURE 1

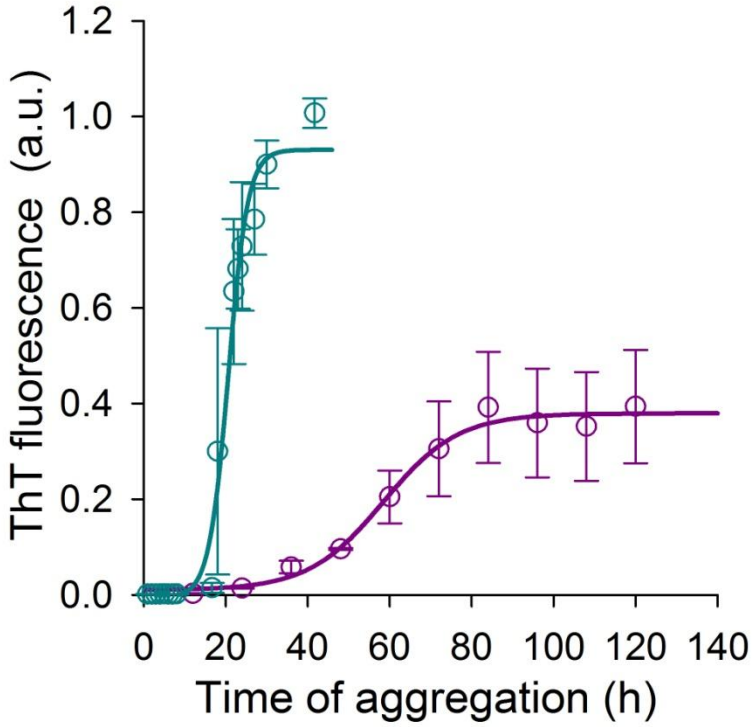

FIGURE 1. ThT accelerates the fibrillation of α-synuclein. ThT fluorescence-monitored kinetics of fibril formation by 100 μM α-synuclein in the absence (purple) and presence (cyan) of 1 mM ThT at pH 7.0, 37 ^{o}C. The error bars represent the standard deviations from three independent aggregation reactions.

FIGURE 2

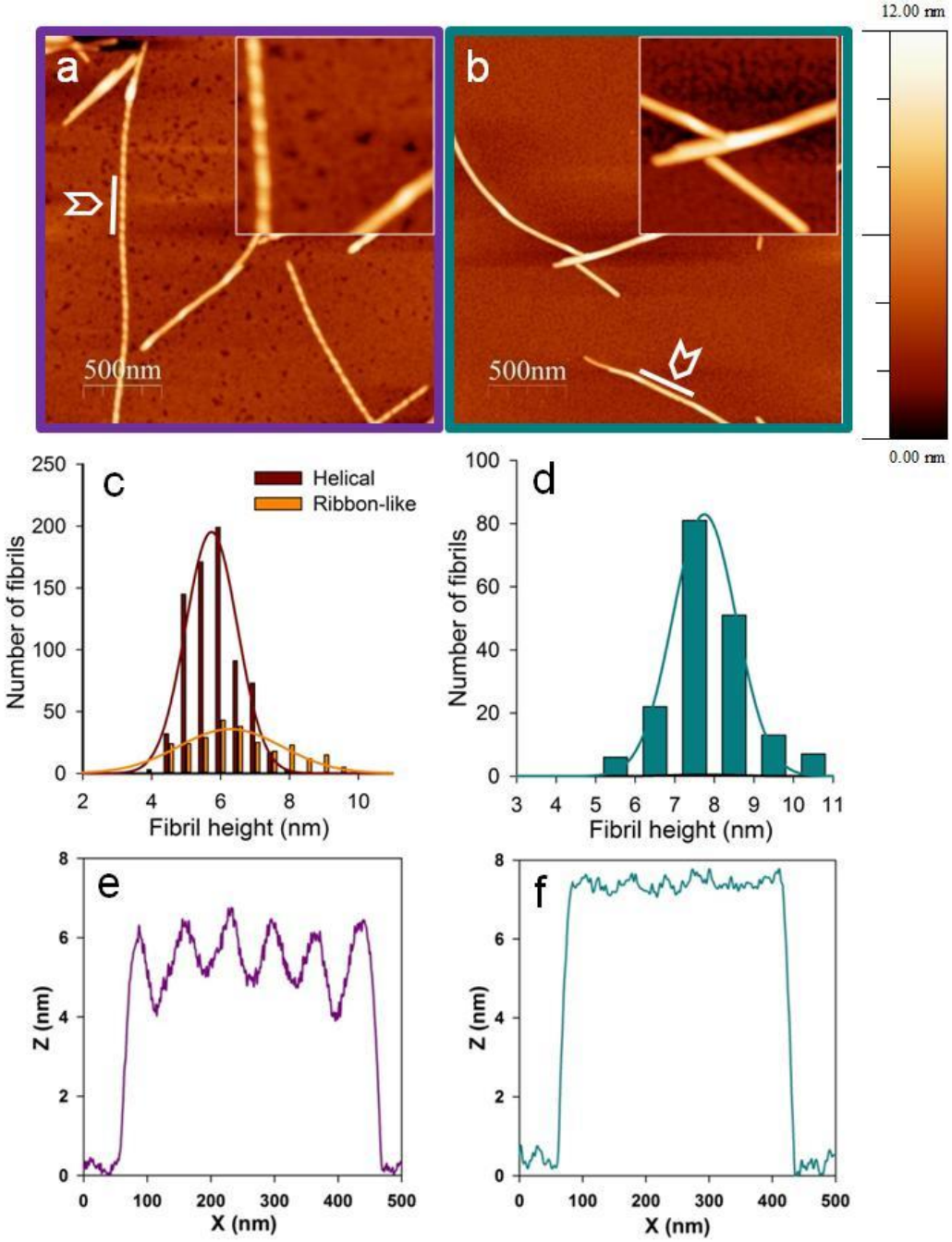

FIGURE 2. Two different morphologies of α-synuclein fibrils are observed in the absence of ThT. AFM images of fibrils formed in (a) the absence of ThT, and (b) the presence of 1 mM ThT at a time corresponding to 3 times the t_{50} of ThT fluorescence-monitored kinetics. Panels c and d show the fibril height distribution from panels a and b, respectively. Panel e shows the height profile of a single helical fibril from panel a; an arrow points to where the height profile is drawn from. Panel f shows the height profile of a single flat, ribbon-like fibril from panel b; an arrow points to where the height profile is drawn from.

FIGURE 3

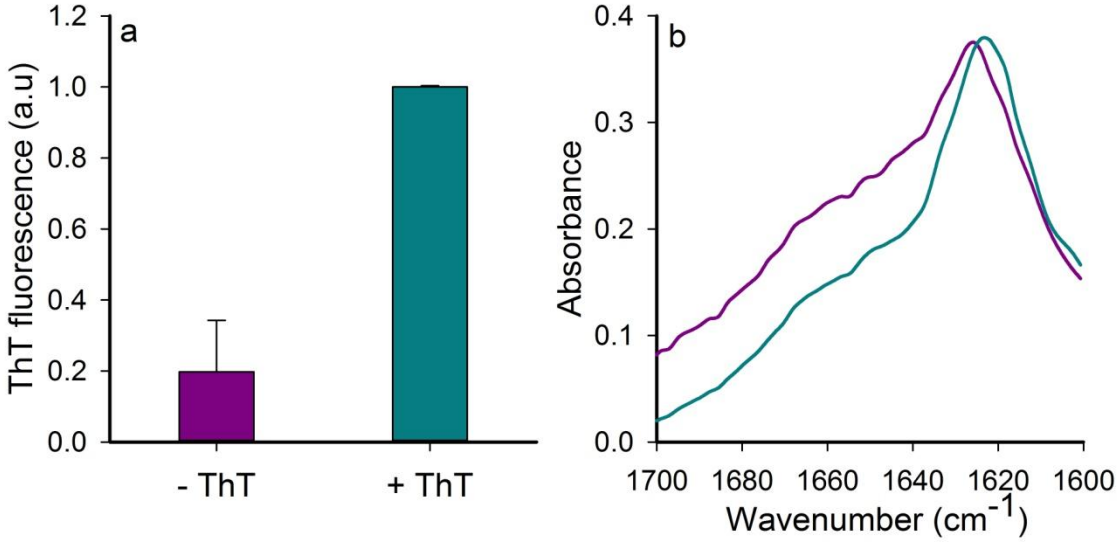

FIGURE 3. Binding of ThT to α-synuclein fibrils and the secondary structure of fibrils. (a) 100 μM fibrils made in the absence and presence of 1 mM ThT were incubated with 1 mM ThT. After washing (see Experimental Procedures) the amount of ThT that remained bound to the fibrils was determined by measurement of ThT fluorescence. The error bars represent the spread from two independent experiments. (b) FTIR spectra of fibrils formed by 100 μM α-synuclein in the absence (purple) and presence (cyan) of ThT. Spectra were acquired at a time corresponding to 3 times the t_{50} of ThT fluorescence-monitored kinetics.

FIGURE 4

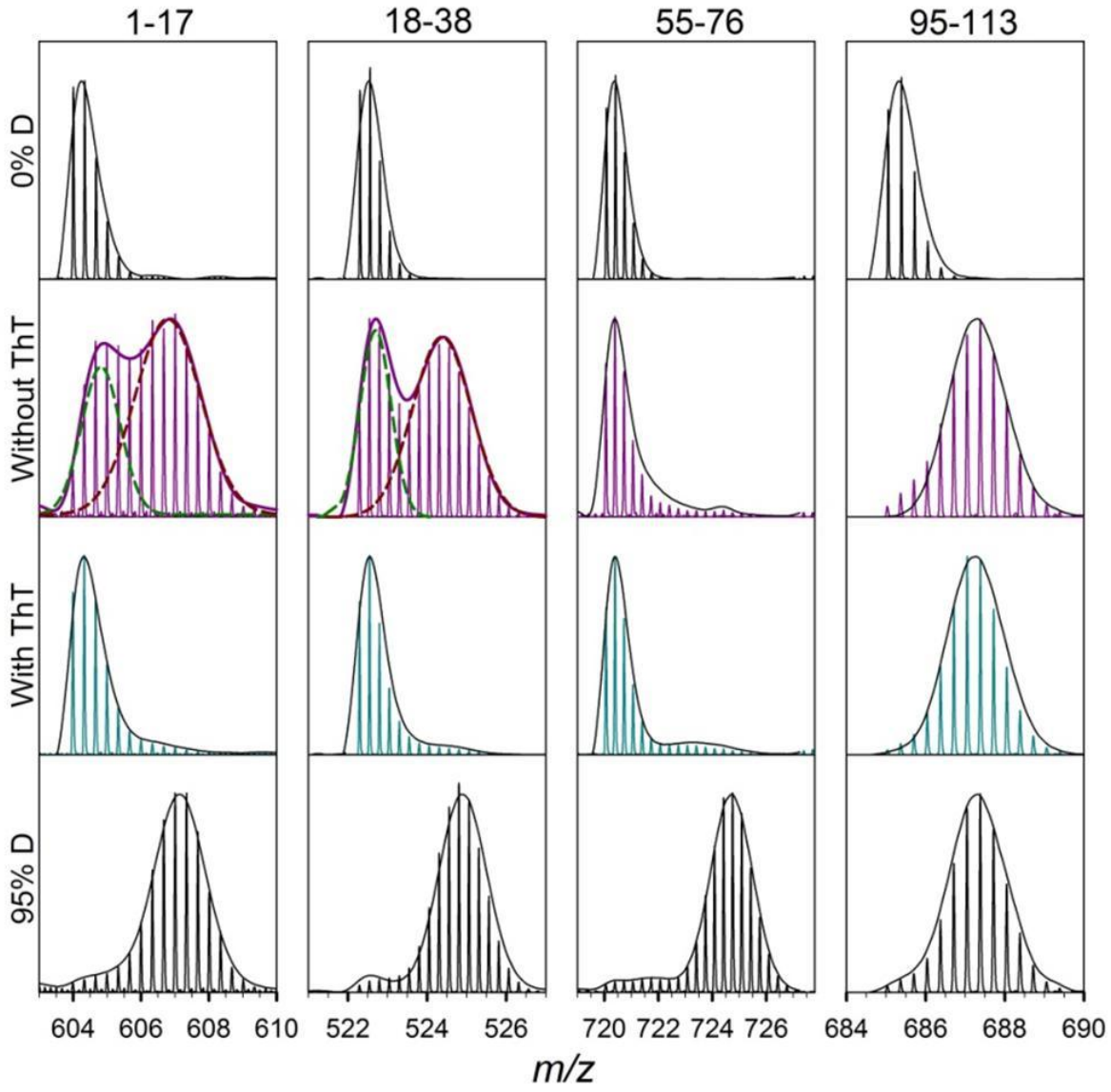

FIGURE 4. Conformational heterogeneity in fibrils formed by α-synuclein. Representative mass spectra of peptide fragments of α-synuclein, for fibrils formed in the absence and presence of 1 mM ThT, along with the mass spectra of protonated (0% D) and deuterated (95% D) controls. Peptide fragments corresponding to sequence segments 1-17 and 18-38 show bimodal mass distributions for fibrils formed in the absence of ThT, and unimodal mass distributions for fibrils formed in the presence of 1 mM ThT.

FIGURE 5

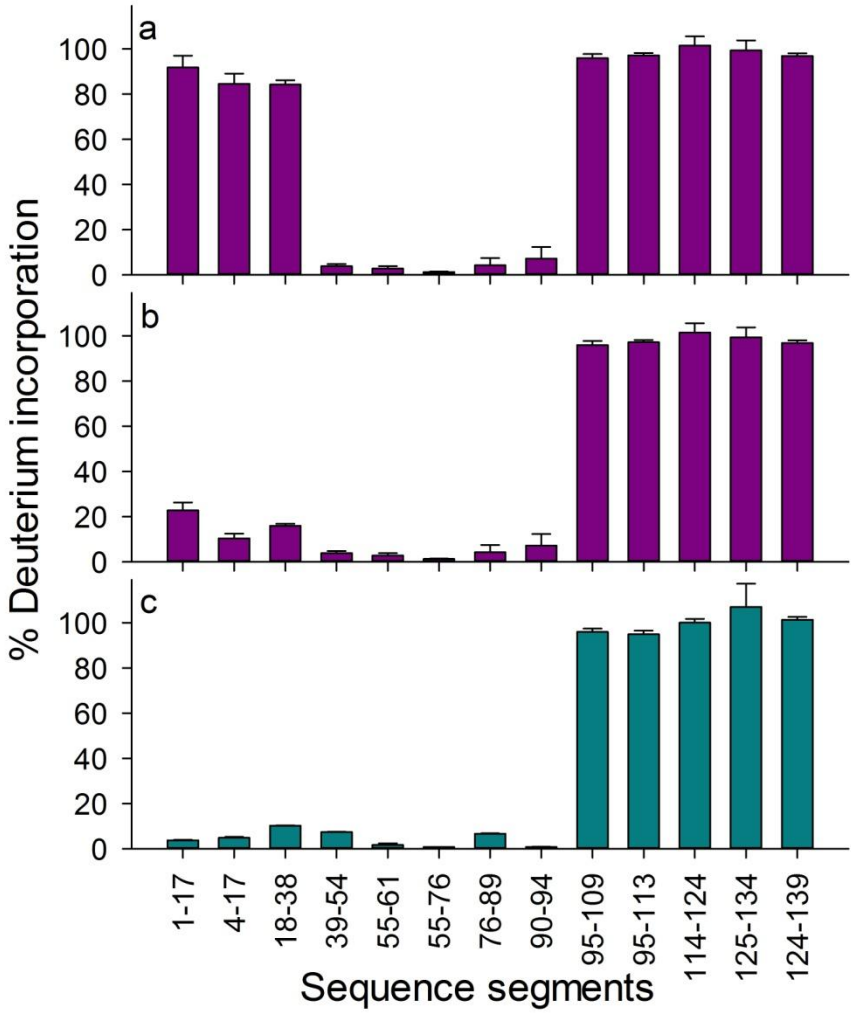

FIGURE 5. The structural core of the α-synuclein fibrils. The percent deuterium incorporation into different sequence segments of fibrils formed by α-synuclein in the absence (a and b) and presence (c) of 1 mM ThT. The deuterium incorporation data for sequence segments 1-17, 4-17 and 18-38 in panel a correspond to the higher mass distribution of the observed bimodal mass distribution, while the data for the same segments in panel b correspond to the lower mass distribution of the observed bimodal distribution. The data in panel c correspond to the unimodal mass distribution observed for the sequence segments for fibrils formed in the presence of 1 mM ThT. The error bars represent the standard deviations from three independent experiments.

FIGURE 6

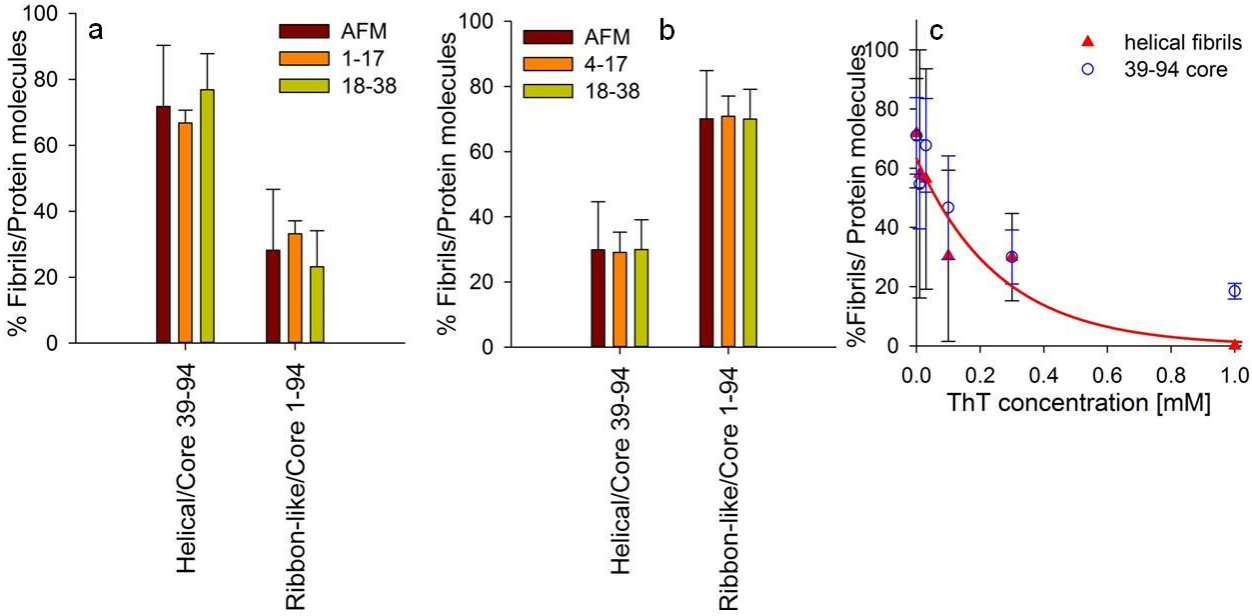

FIGURE 6. Quantification of the two types of fibrils formed by α-synuclein. Panel a shows data for fibrils formed in the absence of ThT. Panel b shows data for fibrils formed in the presence of 0.3 mM ThT. The brown bars represent the percentages of fibrils that were helical and flat, ribbon-like, as determined from counting the fibrils seen in the AFM images. The percentages of protein molecules in fibrils that had and did not have a structural core extending down to residue 1, were determined from the bimodal mass distributions seen for sequence segment 1-17 (orange) and 18-38 (green) as described in the legend to Figure 4. It can be seen that the percentage of fibrillar protein molecules with a core extending down to residue 1 matches the percentage of flat, ribbon-like fibrils formed in both the absence (a) and presence (b) of 0.3 mM ThT. Panel c shows the percentages of fibrillar protein molecules with a core extending from residues 39 to 94, formed at various ThT concentrations, quantified from the higher mass peak of the mass distributions of sequence segment 18-38 (Figure S7). Also shown are the percentages of helical fibrils formed at various ThT concentrations, determined by counting the two types of fibrils seen in AFM images. The red line through the plot of % helical fibril data is described as 63 exp (-3.8 [ThT]). The error bars represent the standard deviations from three independent experiments.

FIGURE 7

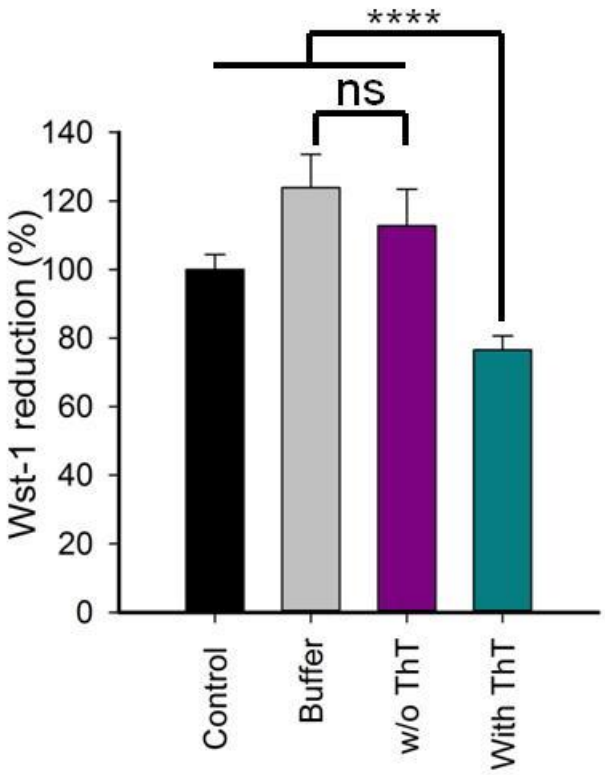

FIGURE 7. Cytotoxicity of α-synuclein fibrils. The cytotoxicity of α-synuclein fibrils (2.5 μM) to HEK-293T cells, was measured using the water-soluble tetrazolium (Wst-1 assay kit). Fibrils were made by incubating 100 μM of α-synuclein at 37 ^{o}C, in the absence and presence of 1 mM ThT. Fibrils were added to a final concentration of 2.5 μM to the cells in each well. The concentration of ThT associated with 2.5 μM fibrils was approximately 0.25 μM .After incubating for 24 h, Wst-1 reagent was added to the wells. After incubating for 2.5 h, the OD at 477 nm was measured. Absorbance data were normalized to that of the untreated cells (Control) having 100% cell viability (ns=non-significant, ****$p<0.0001$ using an unpaired t-test). Buffer represents cells treated with only 1 μM ThT, as described in Experimental Procedures. The error bars represent the standard errors from five independent experiments each with three replicates.

Modulation of the extent of structural heterogeneity in α-synuclein fibrils by the small molecule thioflavin T

Harish Kumar, Jogender Singh, Pratibha Kumari and Jayant B Udgaonkar

J. Biol. Chem. published online July 31, 2017
